Infrared dielectric functions and optical phonons of wurtzite YxAl1-xN (0 less than= x less than= 0.22)

Nabiha Ben Sedrine, Agne Zukauskaite, Jens Birch, Jens Jensen, Lars Hultman, S. Schoeche, M. Schubert and Vanya Darakchieva

Linköping University Post Print

N.B.: When citing this work, cite the original article.

Original Publication:

Nabiha Ben Sedrine, Agne Zukauskaite, Jens Birch, Jens Jensen, Lars Hultman, S. Schoeche, M. Schubert and Vanya Darakchieva, Infrared dielectric functions and optical phonons of wurtzite YxAl1-xN (0 less than= x less than= 0.22), 2015, Journal of Physics D: Applied Physics, (48), 41, 415102.
http://dx.doi.org/10.1088/0022-3727/48/41/415102
Copyright: IOP Publishing: Hybrid Open Access
http://www.iop.org/

Postprint available at: Linköping University Electronic Press
http://urn.kb.se/resolve?urn=urn:nbn:se:liu:diva-122192

Infrared dielectric functions and optical phonons of wurtzite $Y_xAl_{1-x}N$ ($0 \leq x \leq 0.22$)

N. Ben Sedrine[*, 1,2], A. Zukauskaite[1,3], J. Birch[1], J. Jensen[1], L. Hultman[1], S. Schöche[4], M. Schubert[4] and V. Darakchieva[1]

[1] Department of Physics, Chemistry and Biology, Linköping University, SE-58183 Linköping, Sweden

[2] Department of Physics & I3N, University of Aveiro, 3810-193 Aveiro, Portugal

[3] Fraunhofer Institute for Applied Solid State Physics, Tullastr. 72, 79108 Freiburg, Germany

[4] Department of Electrical Engineering, Center for Nanohybrid Functional Materials, University of Nebraska-Lincoln, Lincoln, NE 68588-0511, USA

Abstract

YAlN is a new member of the group-III nitride family with potential for applications in next generation piezoelectric and light emitting devices. In this work we report the infrared dielectric functions and optical phonons of wurtzite (0001) $Y_xAl_{1-x}N$ epitaxial films with $0 \leq x \leq 0.22$. The films are grown by magnetron sputtering epitaxy on *c*-plane Al_2O_3 and their phonon properties are investigated using infrared spectroscopic ellipsometry and Raman scattering spectroscopy. The infrared-active E_1(TO) and LO, and the Raman active E_2 phonons are found to exhibit one-mode behaviour, which is discussed in the framework of the MREI model. The compositional dependencies of the E_1(TO), E_2 and LO phonon frequencies, the high-frequency limit of the dielectric constant, ε_∞, the static dielectric constant, ε_0, and the Born effective charge Z_B are established and discussed.

1. Introduction

Mixed group-IIIA, group-IIIB nitride alloys attract increasing interest due to their unique optoelectronic and piezoelectric properties. A recent theoretical study [1] has shown that alloying ScN with GaN and AlN leads to tunable band gap and polarization in ScAlN and ScGaN alloys, as well as ferroelectricity in $Sc_{0.625}Ga_{0.375}N$. This indicates possible applications of ScAlN and ScGaN alloys in UV and green light-emitting devices, high electron mobility transistors, and ferroelectric and piezoelectric devices. Tuning the optical, electronic and piezoelectric properties of group-III nitride alloys can also be achieved by alloying AlN with

[*] e-mail address: bsnebiha@yahoo.fr

YN [2 - 4]. YN crystallizes in the rock salt structure and is a promising transition nitride material for thermoelectric and thermionic applications. First principle studies have confirmed the semiconductor character of YN [5], however, the YN band gap is largely debated and theoretical values of 0.2 eV [6], 0.49 eV [7], 0.54 eV [8], 0.85 eV [9] and 0.97 eV [10] have been reported. Bibliographic records regarding alloying YN with group-IIIA nitrides are very scarce and mostly experimental studies on $Y_xIn_{1-x}N$ ($0 \leq x \leq 0.094$) [7] thin epitaxial films and theoretical calculations on $(Sc,Y)_{0.5}(Al,Ga,In)_{0.5}N$ [2], $Y_xAl_yGa_{1-x-y}N$ [11] and $Al_xY_yB_{1-x-y}N$ [12] alloys can be found. Orita *et al.* [13] reported the use of YAlN as protective film for improving long-time reliability in semiconductor light-emitting devices. Recently, we have demonstrated the successful synthesis of thin $Y_xAl_{1-x}N$ films on sapphire and Si substrates by reactive magnetron sputtering epitaxy (MSE) [4] and determined the band gap of $Y_xAl_{1-x}N$ ($0 \leq x \leq 0.22$) thin films by spectroscopic ellipsometry [14].

Phonons and dielectric constants are fundamental material parameters and their knowledge is required for device design and optimization. However, no information on the infrared dielectric function (DF) and phonon modes of $Y_xAl_{1-x}N$ exist. In this work, we use infrared spectroscopic ellipsometry (SE) and Raman scattering spectroscopy (RS) to determine the infrared dielectric functions, optical phonons, the high-frequency limit of the dielectric constant, the static dielectric constant and the Born effective charge Z_B of $Y_xAl_{1-x}N$, with x from 0 to 0.22.

2. Experimental details and data analysis

Wurtzite *c*-plane $Y_xAl_{1-x}N$ films (x = 0, 0.02, 0.04, 0.10, 0.13, 0.18 and 0.22) with nominal thicknesses of 300 nm were grown at a temperature of 700°C on *c*-plane $Al_2O_3(0001)$ substrates by reactive DC magnetron sputtering epitaxy in Ar/N_2 mixture. In order to prevent film oxidation, the $Y_xAl_{1-x}N$ were capped with a very thin (nominal thickness of 5 nm) AlN layer. More details about the growth and structural properties of the $Y_xAl_{1-x}N$ can be found elsewhere [4]. The composition and crystal orientation were determined by time of flight energy elastic recoil detection analysis (ToF-E ERDA) and X-ray Diffraction (XRD) using monochromatic Cu Kα1 radiation, respectively [4]. The surface roughness, measured on a similar set of samples, grown on Si (100) substrate, was found to vary between 1 and 5 nm [14].

Spectroscopic ellipsometry (SE) was performed using an infrared variable angle of incidence spectroscopic ellipsometer (IR-VASE, J.A. Woollam Co., Inc.). Data were collected at room temperature, in the spectral region from 400 to 1400 cm^{-1} with a spectral resolution of 2 cm^{-1},

and at 60° and 70° angles of incidence. Raman scattering (RS) spectra in the range of 300 to 900 cm^{-1} were measured with a resolution of 1 cm^{-1} in back-scattering geometry with the film c-axis oriented parallel to the laser beam. The 532 nm laser line with a power of 1 mW was used for excitation.

SE determines the complex reflectance ratio ρ defined in terms of the standard ellipsometric parameters Ψ and Δ as [15]:

$$\rho = \frac{r_p}{r_s} = (\tan\Psi)e^{i\Delta}, \quad (1)$$

where r_p and r_s are the reflection coefficients for light polarized parallel (p) and perpendicular (s) to the sample's plane of incidence, respectively. For the samples studied here, the optical axes of the material constituents are oriented parallel to the surface normal. Therefore, no mode conversion of light p-polarized light to s-polarized light and vice versa occurs and standard ellipsometry can be applied [15, 16].

The IRSE spectra of all samples were analyzed by using a 3-layer model: sapphire substrate /$Y_xAl_{1-x}N$ film/AlN cap layer. The sapphire DF has been previously determined [17], and was used in our work without any changes.
The DF of group-III nitrides can be parameterized by [18]:

$$\varepsilon_j(\omega) = \varepsilon_{\infty,j}\frac{\omega_{LO,j}^2-\omega^2-i\omega\gamma_{LO,j}}{\omega_{TO,j}^2-\omega^2-i\omega\gamma_{TO,j}}, \quad (2)$$

where $j = "\parallel"$ ($j = "\perp"$) for light polarization parallel (perpendicular) to the *c*-axis, with $\omega_{TO,\perp} \equiv \omega_{E1(TO)}$, $\omega_{TO,\parallel} \equiv \omega_{A1(TO)}$, $\omega_{LO,\perp} \equiv \omega_{E1(LO)}$, $\omega_{LO,\parallel} \equiv \omega_{A1(LO)}$ being the respective TO and LO lattice mode frequencies, and $\gamma_{LO,\perp}$, $\gamma_{LO,\parallel}$, $\gamma_{TO,\perp}$, $\gamma_{TO,\parallel}$ the respective phonon broadening parameters. $\varepsilon_{\infty,\perp}$ and $\varepsilon_{\infty,\parallel}$ are the high-frequency limit dielectric constants for the two respective polarizations.
Due to the relatively small film thickness, the IRSE data do not have enough sensitivity to distinguish between E_1(LO) and A_1(LO) phonons. Therefore, the following parameters are treated isotropically: $\omega_{E1(LO)} = \omega_{A1(LO)}$, $\gamma = \gamma_{LO} = \gamma_{TO}$ where $\gamma_{LO} = \gamma_{LO,\perp} = \gamma_{LO,\parallel}$, $\gamma_{TO} = \gamma_{TO,\perp} = \gamma_{TO,\parallel}$, and $\varepsilon_{\infty,\perp} = \varepsilon_{\infty,\parallel} = \varepsilon_\infty$. Due to the *c*-plane orientation of the YAlN layers, the ellipsometry data are not sensitive to the TO mode frequency with polarization vector parallel to the sample normal [16,19]. Consequently, the A_1(TO) phonon mode frequency of 611 cm^{-1} [20] was taken as fixed parameter in the IRSE analysis of all $Y_xAl_{1-x}N$ samples. We have

carefully checked that such assumption does not affect the best-match results of the phonon parameters and dielectric constants.

The AlN DF as determined for the yttrium-free film was used for the parameterization of the DF of the AlN cap layer in the data analysis for all samples. The cap layer thickness was kept fixed to the nominal value of 5 nm. The frequency and broadening parameters of the LO and E_1(TO) phonon frequencies, as well as ε_∞, and the $Y_xAl_{1-x}N$ layer thickness, were varied simultaneously in order to match model calculated data as closely as possible to the experimental data.

3. Results and discussion

The XRD results show that all $Y_xAl_{1-x}N$ films, have wurtzite crystal structure with their *c*-axis [0001] being parallel to the growth direction. Pole figure measurements (not shown here) reveal the epitaxial nature of the films with unique azimuthal orientation of the (0002) crystallites up to x=0.22. Figure 1 (a) shows normalized XRD 2θ-ω scans in the vicinity of the $Y_xAl_{1-x}N$ (0002) diffraction peak for all the films. The (0002) peak shifts towards lower angles from 36° to 34.4° and broadens as yttrium content increases. The peak shift is related to the increase of the *c*-lattice parameter as shown in Fig. 1(b). The ionic radius of Y is larger than Al, which can explain the observed increase in the lattice parameter with increasing Y content. Our result [Fig. 1(b)] is also in excellent agreement with the theoretical predictions of the lattice parameters of wurtzite $Y_xAl_{1-x}N$ solid solutions in this composition range [4]. The observed broadening of the (0002) peak with increasing yttrium content is related to a decrease of the vertical coherence length. The later may be associated with increased defect densities and alloy disorder. In addition, for $x \geq 0.10$ a second low-intensity peak appears at about $2\theta \approx 37°$, which can be assigned to diffraction from wurtzite $Y_xAl_{1-x}N$ (10-11) crystallographic planes. Another low-intensity peak appears at lower 2θ angles below 32°, which we assign to diffraction from wurtzite $Y_xAl_{1-x}N$ (10-10) crystallographic planes.

Figure 2 shows the experimental and best-match model IRSE ψ [Fig. 2 (a)] and Δ [Fig. 2 (b)] spectra of the $Y_xAl_{1-x}N$ films and the sapphire substrate at incidence angle of 70°. An excellent agreement between experimental (dash dotted lines) and model calculated data (solid lines) is seen, which confirms that the model used in this study gives a good fit quality for the $Y_xAl_{1-x}N$ films. Fig. 3 depicts the imaginary part of the dielectric function $\mathrm{Im}(\varepsilon)$ [Fig. 3 (a)] and the imaginary part of the dielectric loss functions $\mathrm{Im}(-1/\varepsilon)$ [Fig. 3 (b)] obtained from the model line shape analysis. The frequencies of the TO modes [indicated by arrows in Fig. 3 (a)]

correspond to the poles of the dielectric function ε, and the ones of the LO modes [indicated by arrows in Fig. 3 (b)] correspond to the poles of the dielectric loss function (1/ε). Table I summarizes the best-match model parameters of $Y_xAl_{1-x}N$ ε_∞, LO and E_1(TO) phonon frequencies and broadening parameters obtained from the IRSE data analysis.

The IRSE data analysis renders one-mode behaviour for the IR active phonons of $Y_xAl_{1-x}N$ in the studied yttrium content range ($0 \leq x \leq 0.22$), i.e. one TO-LO phonon pair is sufficient to describe the $Y_xAl_{1-x}N$ IR dielectric function (eq. 2). The optical phonon mode behaviour in a ternary $A_xB_{1-x}C$ is conventionally categorized into two main classes referred to as one- and two-mode behaviour. In the case of one-phonon mode behaviour, the alloy only exhibits one set of TO and LO frequencies, which change continuously and usually nearly linearly with composition from the respective frequencies of the binary AC compound to those of the BC compound. On the other hand, the two-phonon mode behaviour is described by two energetically well-separated sets of phonon mode pairs. The first set of phonon pair occurs at frequencies close to those of the binary compound AC, while the second phonon pair occurs at frequencies close to the respective phonons of the binary compound BC. The compositional dependences in this case are more complex.

In order to predict whether an alloy $A_xB_{1-x}C$ will show one- or two-mode behaviour, the modified random element isodisplacement (MREI) model was proposed by Chang and Mitra [21,22]. According to the MREI model, for an alloy to exhibit two-mode behaviour, the following relationship must be fulfilled: $M_{A(B)} < \mu_{BC(AC)}$, where $\frac{1}{\mu_{BC}} = \frac{1}{M_B} + \frac{1}{M_C}$, with M being the atomic mass and μ -the reduced mass. In contrast, if $M_{A(B)} > \mu_{BC(AC)}$, the alloy should show one-mode behaviour. The MREI model predicts one-mode behaviour for $Y_xAl_{1-x}N$ alloy, since the atomic mass of yttrium (M_Y) is larger than the reduced mass of AlN ($M_{Y,Al} > \mu_{AlN,YN}$, where $\frac{1}{\mu_{AlN}} = \frac{1}{M_{Al}} + \frac{1}{M_N}$ and $\frac{1}{\mu_{YN}} = \frac{1}{M_Y} + \frac{1}{M_N}$), which is in accordance with our IRSE results. Similarly, in other group-III nitride alloys such as $In_xGa_{1-x}N$ [23] and $Sc_xAl_{1-x}N$ [24] (where the atomic mass of indium/scandium is larger than the reduced mass of GaN/AlN), one-phonon mode behaviour was experimentally demonstrated over the entire composition range of $In_xGa_{1-x}N$, and for $x \leq 0.16$ for $Sc_xAl_{1-x}N$.

The arrows in Fig. 2 indicate the positions of the $Y_xAl_{1-x}N$ LO and E_1(TO) phonon frequencies, which mark the YAlN band of total reflection. For the AlN film, the E_1(TO) and LO phonon frequencies are 666 and 887 cm^{-1}, respectively. These values agree well with previously published data for the respective phonon frequencies in high-quality single crystalline wurtzite

AlN films with rocking curve widths as low as 12 arcsec [25] and bulk AlN [26]. It is seen from Fig. 2 that the low-frequency edge of the YAlN band of total reflection becomes less steep with increasing the yttrium content. This is a result of the significant increase of the E_1(TO) phonon broadening parameter and the phonon red-shift as seen in Fig. 3 (a) (see also Table I). Likewise, an increased broadening could also be seen for the LO phonon [Fig. 3 (b)]. The observed increase of the phonon broadening can be associated with an increase of defect densities and alloy disorder as inferred from XRD.

Figure 4 shows the Raman spectra of the $Y_xAl_{1-x}N$ layers in the range 300 - 900 cm^{-1}. The allowed YAlN E_2 mode (see the inset) and a number of sapphire peaks (indicated with asterisks) can be well resolved. The E_2 phonon frequency of 655.2 cm^{-1} for the AlN film is in good agreement with the previously reported results for high-quality AlN single crystals [27]. For the films with yttrium content above x=0.10, the E_2 peak becomes too weak and broadens significantly, which does not allow precise determination of its frequency. Table I also includes the E_2 phonon frequencies, and the corresponding broadening parameters, obtained from the Raman scattering measurements. Similar to the LO and E_1(TO) modes, a one-mode behaviour is also observed for the Raman active E_2 mode.

The phonon mode frequencies obtained from the IRSE and RS are plotted as a function of the yttrium content in Fig. 5. A linear decrease of the phonon frequencies with increasing yttrium content is found. The LO, E_1(TO) and E_2 phonon frequency dependencies are determined to be:

LO: $\omega_{LO}(x) = 898\ cm^{-1} - 251 \bullet x\ cm^{-1}$, and

E_1(TO): $\omega_{E1(TO)}(x) = 665\ cm^{-1} - 367 \bullet x\ cm^{-1}$ for $0 \leq x \leq 0.18$, and

E_2: $\omega_{E2}(x) = 654\ cm^{-1} - 260 \bullet x\ cm^{-1}$ for $0 \leq x \leq 0.10$.

The observed phonon softening with increasing yttrium content is attributed to an increase in the metal ion mass and an increase of the dynamic effective charge as discussed below.

The $Y_xAl_{1-x}N$ film with the highest yttrium content of x=0.22 shows blue-shifts of the LO and E_1(TO) phonon frequencies with respect to the corresponding values in $Y_xAl_{1-x}N$ film with $x \leq 0.18$. These blue-shifts might be due to a lower yttrium content than the one provided from ERDA, which gives an average value over all crystallites. In fact, as can be seen from Fig. 1 (a), the (0002) peak position corresponding to the film with x=0.22 is slightly higher than the one corresponding to the respective peak of the film with x=0.18. This is also reflected in a smaller *c*-lattice parameter [Fig. 1 (b)] for the film with x=0.22 compared to the film with

x=0.18. On the other hand, the additional peaks associated with diffraction from the (10-11) and (10-10) crystallographic planes are red-shifted for the film with x=0.22 with respect to the ones for the film with x=0.18. This can be associated with different lattice parameters of the crystallites with different crystallographic orientations. Since the lattice parameters are directly related to composition and strain, a spread in composition or/and strain may be inferred for the $Y_xAl_{1-x}N$ film with the highest yttrium content. Such composition/strain effects might explain the observed slight blue-shift of the phonon mode frequencies with increasing yttrium content. In principle, short-order effects, such as defect states or clustering, may also affect the complex DF and optical phonons, respectively. Note that the linear dependences of both lattice parameters (this work) and band gap energies [14] with x strongly suggest that the $Y_xAl_{1-x}N$ films behave as a solid solution for the compositional range studied. These trends are also consistent with the results from first principle calculations for random $Y_xAl_{1-x}N$ alloys with wurtzite structure [4] suggesting that short-range effects are not likely to play a major role.

AlN has a wurtzite crystal structure, while YN on the other hand has a rocksalt crystal structure, and a transition between wurtzite and rocksalt structures is expected to occur for $Y_xAl_{1-x}N$ with $x \sim 0.75$ according to recent *ab initio* calculations [4]. It is important to note that all $Y_xAl_{1-x}N$ films studied here have wurtzite structure. To the best of our knowledge, no experimental data have been reported for the YN phonon frequencies. Saha *et al.* [10] reported 165 cm^{-1} and 500 cm^{-1} for the TO and LO phonons respectively by using density functional theory (DFT) in the generalized gradient approximation GGA+U and GW approximations. Very recently, Yurdasan *et al.* [28] reported 362 cm^{-1} and 549 cm^{-1} for TO and LO phonons, respectively, by using DFT plane-wave pseudopotential calculations. These YN theoretical phonon frequencies are included in Figure 5 for illustration. The observed decrease of the experimental phonon frequencies with increasing yttrium content is expected in view of the YN phonon frequencies (see Fig. 5).

Figure 6 shows the high-frequency limit dielectric constant ε_∞ obtained from the IRSE analysis as well as the static dielectric constant ε_0 obtained from the Lyddane-Sachs-Teller relation: $\varepsilon_0 = \varepsilon_\infty (\frac{\omega_{LO}}{\omega_{TO}})^2$ (Table I), as function of yttrium content x. The ε_∞ value of 3.78, for the film with x=0, is in good agreement with the reported data for high-quality wurtzite AlN [25]. It is seen from Fig. 6 that ε_∞ and ε_0 show an overall linear increase with increasing yttrium content, with

$\varepsilon_\infty(x) = 3.7 + 5.5 \bullet x$ and

$\varepsilon_0(x) = 6.9 + 11.4 \bullet x$.

The observed trend in ε_∞ is consistent with the value of 13.1 predicted for YN ε_∞ [10]. The increase in ε_∞ with increasing Y content can be qualitatively understood as a result of the decrease of the $Y_xAl_{1-x}N$ band gap from 6.2 eV for x = 0 down to 4.5 eV for x = 0.22 [4, 14]. Consequently, an enhanced intermixing of valence and conduction band states, causing stronger electronic polarization takes place with increasing Y. Similar effect has also been recently observed for ScAlN [24]. We note that the variation of ε_∞ with x in $Y_xAl_{1-x}N$ is considerably steeper compared to the respective trend in ScAlN [24]. This indicates that similar variations of dielectric constant and refractive index can be reached by lower alloying contents of Y as compared to ScAlN.

We also calculated the Born effective charge Z_B in $Y_xAl_{1-x}N$:

$$4\pi^2(\omega_{LO}^2 - \omega_{E1(TO)}^2) = \frac{2Z_B^2e^2}{\varepsilon_0^*\varepsilon_\infty V_0}\left(\frac{1}{M_{metal}} + \frac{1}{M_N}\right) \quad (3)$$

where e is the elementary charge, ε_0^* is the vacuum permittivity, V_0 is the unit cell volume, ε_∞ is the high-frequency limit of the dielectric constant, M_{metal} and M_N are the atomic ion masses such as $M_{metal} = (1-x)M_{Al} + xM_Y$. The V_0 is calculated from the measured c-lattice parameters [Fig. 1 (b)] and the estimated a-lattice parameters obtained from our previously reported $(c/a)_{calc}$ ratio [4]. The ω_{LO} and $\omega_{E1(TO)}$ are the LO and E_1(TO) phonon frequencies obtained from the IRSE analysis. The results are presented in Fig. 6 and Table 1.

The Born effective charge provides a quantitative measure of the ionic character of the metal-N bond. $Z_B = 2.3$ is calculated for AlN (Fig. 6) which is somehow lower than the previously reported values of 2.47 - 2.53 from experiments and calculations [24, 29]. A Z_B value lower than 3 for AlN is consistent with the partly covalent character of the bonding in AlN [25]. Alloying with Y leads to a linear increase of Z_B:

$Z_B(x) = 2.30 + 3.27 \bullet x$.

This increase is attributed to a stronger ionic bonding character in YN compared to AlN and it is consistent with the theoretical predictions for the Born effective charge in YN of 4.50 and 4.77 [30]. A linear extrapolation of the data in Fig. 6 renders $Z_B = 5.58$ for YN which is higher than the values predicted by theory [30]. Internal strain due to the large disparity of atomic sizes of Y and Al could provide a possible explanation for the observed differences. However, further effects such as different compositional dependencies for wurtzite and rock-salt $Y_xAl_{1-x}N$ may also play an important role. Additional uncertainties in the $Y_xAl_{1-x}N$ Born effective charge values may stem from the fact that Eq.3 is strictly valid for random alloys. In this respect, we

note the excellent agreement of the composition dependencies of the lattice parameters (Fig. 1b) with the theoretical predictions for random $Y_xAl_{1-x}N$ alloys with wurtzite structure [4]. The linear dependence of the band gap energies of our films [14] also indicates that $Y_xAl_{1-x}N$ behaves as a solid solution for the compositional range studied. However, more experimental and theoretical works are called for to further elucidate the short-range effects in the $Y_xAl_{1-x}N$ alloy system.

4. Conclusions

We have determined the infrared dielectric function and phonon mode parameters of wurtzite *c*-plane $Y_xAl_{1-x}N$ ($0 \leq x \leq 0.22$) films grown by magnetron sputtering epitaxy on $Al_2O_3(0001)$ substrates. The E_1(TO), E_2 and LO phonon modes are found to exhibit one-mode behaviour for the compositional range studied in good agreement with the MREI model predictions. All phonon modes exhibit red-shifts with increasing x described by: $\omega_{LO}(x)$ = 898 cm^{-1} - 251•x cm^{-1}, $\omega_{E1(TO)}(x)$= 665 cm^{-1} - 367•x cm^{-1} for $0 \leq x \leq 0.18$, and $\omega_{E2}(x)$= 654 cm^{-1} - 260•x cm^{-1} for $x \leq 0.10$. The phonon softening with increasing yttrium content is attributed to an increase in the metal ion mass and an increase of the dynamic effective charge. At high yttrium content x = 0.22, a deviation from the linear compositional trend is observed and attributed to strain and compositional variations in crystallites with different orientations. The high-frequency limit of the dielectric constant ε_∞ and the static dielectric constant ε_0, are determined and are found to increase with increasing yttrium content with $\varepsilon_\infty(x)$ = 3.7 + 5.5•x and $\varepsilon_0(x)$ = 6.9 + 11.4•x. The Born effective charge Z_B is calculated and found to increase with increasing yttrium content $Z_B(x)$ = 2.30 + 3.27•x. This is attributed to an increase of the metal-N bond and internal strain. These results can be used in future works on the design, modeling and fabrication of piezoelectric and optoelectronic devices based on YAlN and related alloys.

Acknowledgements

We acknowledge financial support from the Swedish Research Council (VR) under grant No.2013-5580, the Swedish Governmental Agency for Innovation Systems (VINNOVA) under grant No.2011-03486, and the Swedish Foundation for Strategic Research (SSF) under grant No.2012FFL12-0181. Financial support from the National Science Foundation is acknowledged under Award Nos. MRSEC DMR-0820521 and EPS-1004094. N. Ben Sedrine acknowledges partial financial support from the project RECI/FIS-NAN/0183/2012 (FCOMP-

01-0124-FEDER-027494) and Stiftelsen Lars Hiertas Minne (FO2013-0587). Dr. V. Stanishev is acknowledged for fruitful discussions.

References

[1] S. Zhang, D. Holec, W. Y. Fu, C. J. Humphreys, and M. A. Moram, J. Appl. Phys. 114, 133510 (2013)

[2] C. Tholander, I. A. Abrikosov, L. Hultman, and F. Tasnádi, Phys. Rev. B 87, 094107 (2013).

[3] J. P. Dismukes and T. D. Moustakas: Proc.-Electrochem. Soc. 96-11, 110 (1996).

[4] A. Zukauskaite, C. Tholander, J. Palisaitis, Per O. Å. Persson, V. Darakchieva, N. Ben Sedrine, F. Tasnádi, B. Alling, J. Birch, L. Hultman: J. Phys. D: Appl. Phys. 45, 422001 (2012).

[5] Y. Cherchab, B. Amrani, N. Sekkal, M. Ghezali, K. Talbi, Physica E, 40, 606 (2008).

[6] L. Mancera, J. A. Rodriguez, and N. Takeuchi, J. Phys. Condens. Matter 15, 2625 (2003).

[7] C. N. Zoita, M. Braic, and V. Braic: Dig. J. Nanomater. Biostruct. 6 4 1877 (2011).

[8] L. Tie-Yu, H. Mei-Chun, Chin. Phys. 16, 62 (2007).

[9] C. Stampfl, W. Mannstadt, R. Asahi, and A. J. Freeman, Phys. Rev. B 63, 155106 (2001).

[10] B. Saha, T. D. Sands, and U. V. Waghmare, J. Appl. Phys. 109, 073720 (2011).

[11] K. Shimada, A. Zenpuku, K. Fujiwara, K. Hazu, S. F. Chichibu, M. Hata, H. Sazawa, T. Takada, and T. Sota, J. Appl. Phys. 110, 074114 (2011).

[12] B. Ghebouli, M. A. Ghebouli, M. Fatmi, Physica B 406, 2521 (2011).

[13] K. Orita and S. Yoshida, US 2010/0314653 A1 patent

[14] N. Ben Sedrine, A. Zukauskaite, J. Birch, L. Hultman and V. Darakchieva, Jpn. J. Appl. Phys. 52, 08JM02 (2013).

[15] H. Fujiwara: Spectroscopic ellipsometry: principles and applications. Wiley, Chichester (2007).

[16] M. Schubert, “Infrared Ellipsometry on semiconductor layer structures: Phonons, plasmons and polaritons”, Springer (2004).

[17] M. Schubert, T. E. Tiwald, and C. M. Herzinger, Phys. Rev. B 61, 8187 (2000).

[18] V. Darakchieva, phys. stat. sol. (a), 205, 905 (2008).

[19] A. Kasic, M. Schubert, S. Einfeldt, D. Hommel, and T. E. Tiwald, Phys. Rev. B, 62, 7365 (2000).

[20] V. Yu. Davydov, Yu. E. Kitaev, I. N. Goncharuk, A. N. Smirnov, J. Graul, O. Semchinova, D. Uffmann, M. B. Smirnov, A. P. Mirgorodsky, and R. A. Evarestov, Phys. Rev. B, 58, 12899 (1998).

[21] I. F. Chang and S. S. Mitra, Phys. Rev. 172, 924 (1968).
[22] H. Grille, C. Schnittler, and F. Bechstedt, Phys. Rev. B 61, 6091 (2000).
[23] S. Hernàndez, R. Cuscó, D. Pastor, L. Artús, K. P. O'Donnell, R. W. Martin, I. M. Watson, Y. Nanishi, and E. Calleja, J. Appl. Phys. 98, 013511 (2005).
[24] R. Deng, K. Jiang and D. Gall, J. Appl. Phys. 115, 013506 (2014).
[25] V. Darakchieva, J. Birch, M. Schubert, T. Paskova, S. Tungasmita, G. Wagner, A. Kasic, and B. Monemar, Phys. Rev. B 70, 045411 (2004).
[26] G. Callsen, M. R. Wagner, J. S. Reparaz, F. Nippert, T. Kure, S. Kalinowski, A. Hoffmann, M. J. Ford, M. R. Phillips, R. F. Dalmau, R. Schlesser, R. Collazo, and Z. Sitar, Phys. Rev. B 90, 205206 (2014).
[27] J. G. Tischler and J. A. Freitas, Jr. Appl. Phys. Lett. 85, 1943 (2004).
[28] N. B. Yurdasan, S. E. Gulebaglan, G. B. Akyuz, Acta Pysica Polonica A, 123, Issue 2, 317 (2013).
[29] J. M. Wagner and F. Bechstedt, Phys. Rev. B66, 115202 (2002).
[30] S. Tahri, A. Qteish, I. I Al-Qasir, and N. Meskini, J. Phys.: Condens. Matter 24, 035401 (2012).

Table I: $Y_xAl_{1-x}N$ films best-match layer thickness and IRSE DF parameters: ε_∞, ε_0, Z_B, ω_{LO}, $\omega_{E1(TO)}$ and γ for the $Y_xAl_{1-x}N$/sapphire. ω_{E2} and γ_{E2} obtained from Raman scattering measurements are also included. Error bars in parenthesis correspond to the 90% confidence limits.

x	$Y_xAl_{1-x}N$ Thickness (nm)	ε_∞	ε_0	Z_B	ω_{LO} (cm^{-1})	$\omega_{E1(TO)}$ (cm^{-1})	γ (cm^{-1})	ω_{E2} (cm^{-1})	γ_{E2} (cm^{-1})
0	260 (2)	3.78 (0.01)	6.70	2.25	886.9 (0.6)	666.0 (0.1)	15.6 (0.2)	655.2 (0.2)	9.1 (0.2)
0.02	269 (2)	3.84 (0.02)	7.04	2.38	899.7 (0.6)	664.2 (0.2)	59.7 (0.3)	649.3 (0.5)	20.0 (0.8)
0.04	311 (2)	4.04 (0.01)	7.57	2.48	894.1 (0.5)	653.1 (0.2)	47.6 (0.2)	642.2 (0.5)	22.8 (0.5)
0.10	245 (2)	4.24 (0.02)	8.11	2.61	873.2 (0.7)	631.0 (0.5)	108.3 (0.8)	629.0 (0.5)	95 (37)
0.13	293 (1)	4.50 (0.01)	9.11	2.80	862.4 (0.6)	605.8 (0.5)	90.9 (0.8)	--	--
0.18	236 (3)	4.56 (0.03)	8.69	2.86	852.7 (0.8)	617.4 (0.9)	121.2 (1.3)	--	--
0.22	219 (4)	5.14 (0.05)	9.28	3.01	870.0 (1.1)	647.3 (1.1)	138.5 (1.7)	--	--

Figure Captions

Fig. 1: Normalized XRD 2θ-ω scans of $Y_xAl_{1-x}N$ with $0 \leq x \leq 0.22$ [Fig. 1(a)] and *c*-lattice parameter as a function of yttrium content [Fig. 1(b)], the error bars are smaller than the symbol size and could not be plotted.

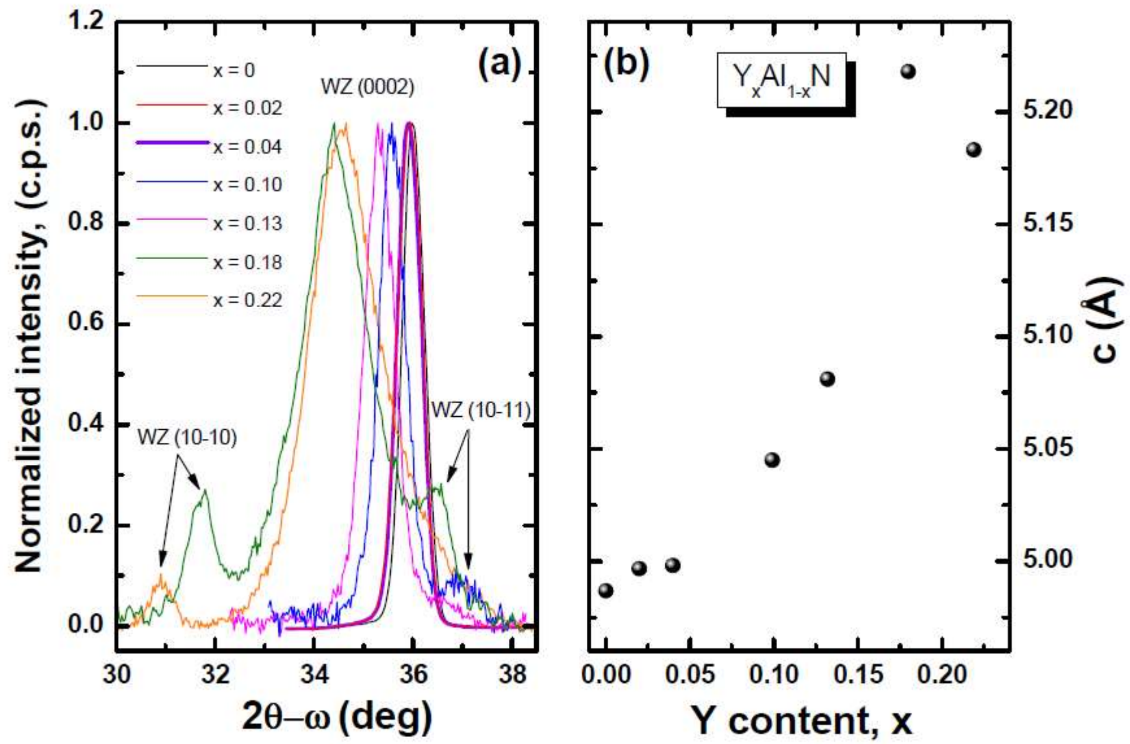

Fig. 2: Experimental (dash dots) and best-match calculated (solid lines) IRSE ψ [Fig. 2(a)] and Δ [Fig. 2(b)] spectra of the $Y_xAl_{1-x}N$ films on sapphire substrate at incidence angle $\Phi = 70°$. Arrows indicate the positions of the $Y_xAl_{1-x}N$ E_1(TO) and LO phonon modes.

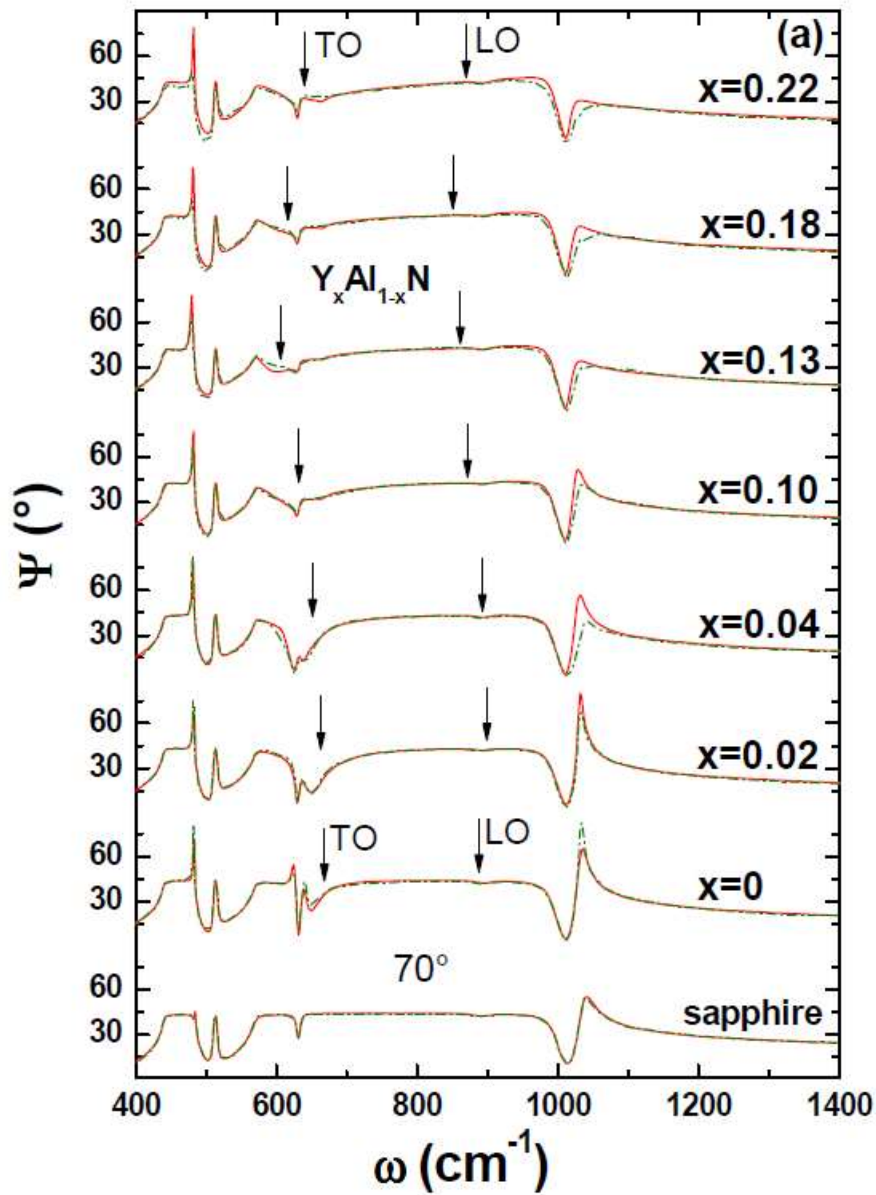

Fig. 2 (a)

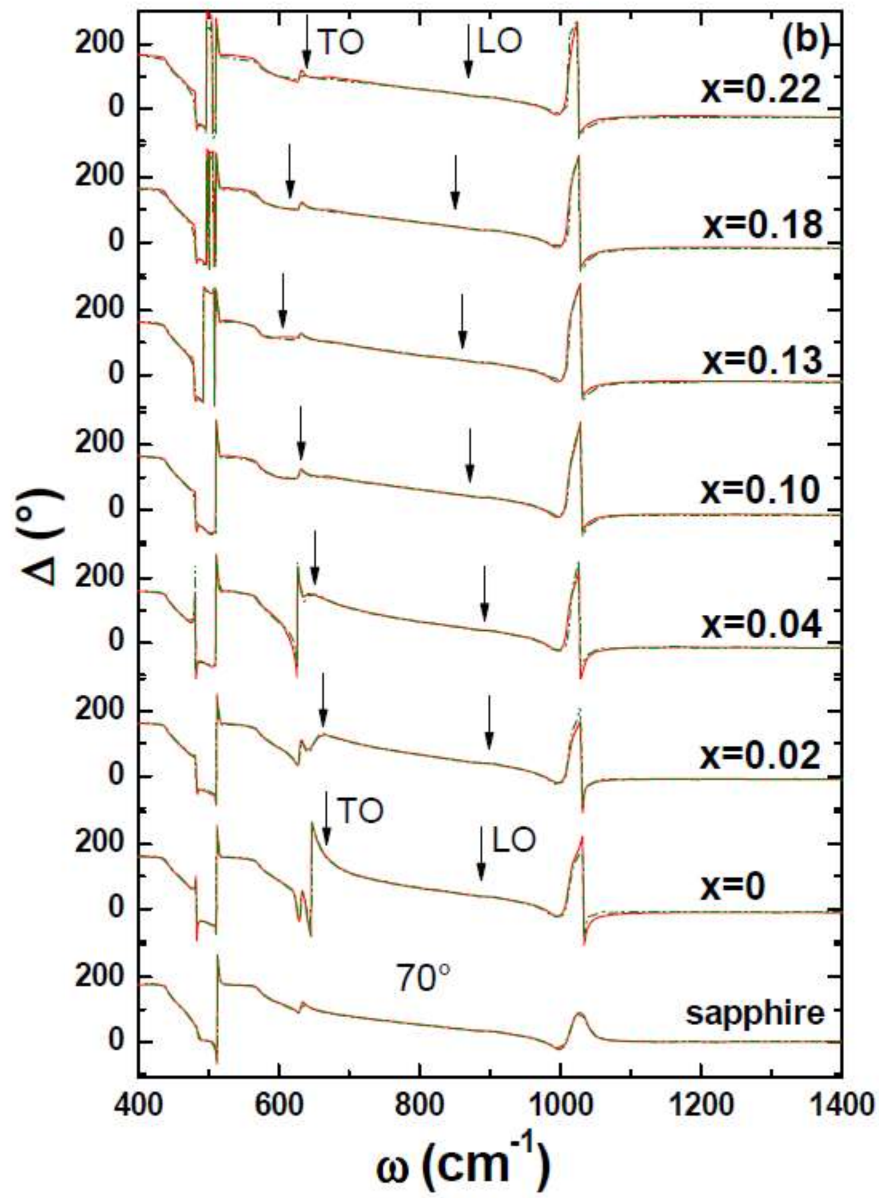

(b)
TO
LO
x=0.22
x=0.18
x=0.13
x=0.10
x=0.04
x=0.02
TO
LO
x=0
70°
sapphire
Δ (°)
ω (cm-1)

Fig. 3: Imaginary part of the dielectric function $\mathrm{Im}(\varepsilon)$ (a) and the imaginary part of the dielectric loss functions $\mathrm{Im}(-1/\varepsilon)$ (b) obtained from the model line shape analysis.

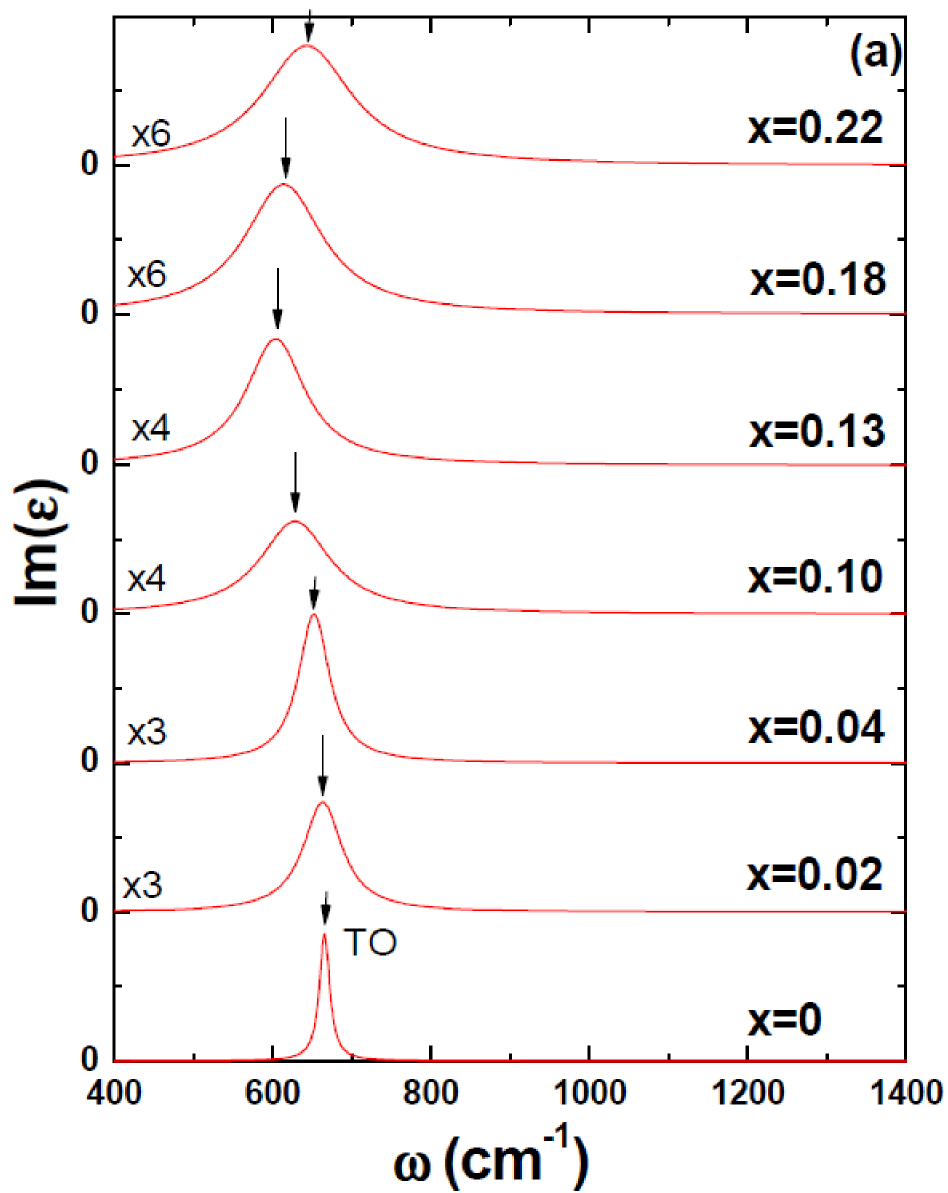

Fig. 3 (a)

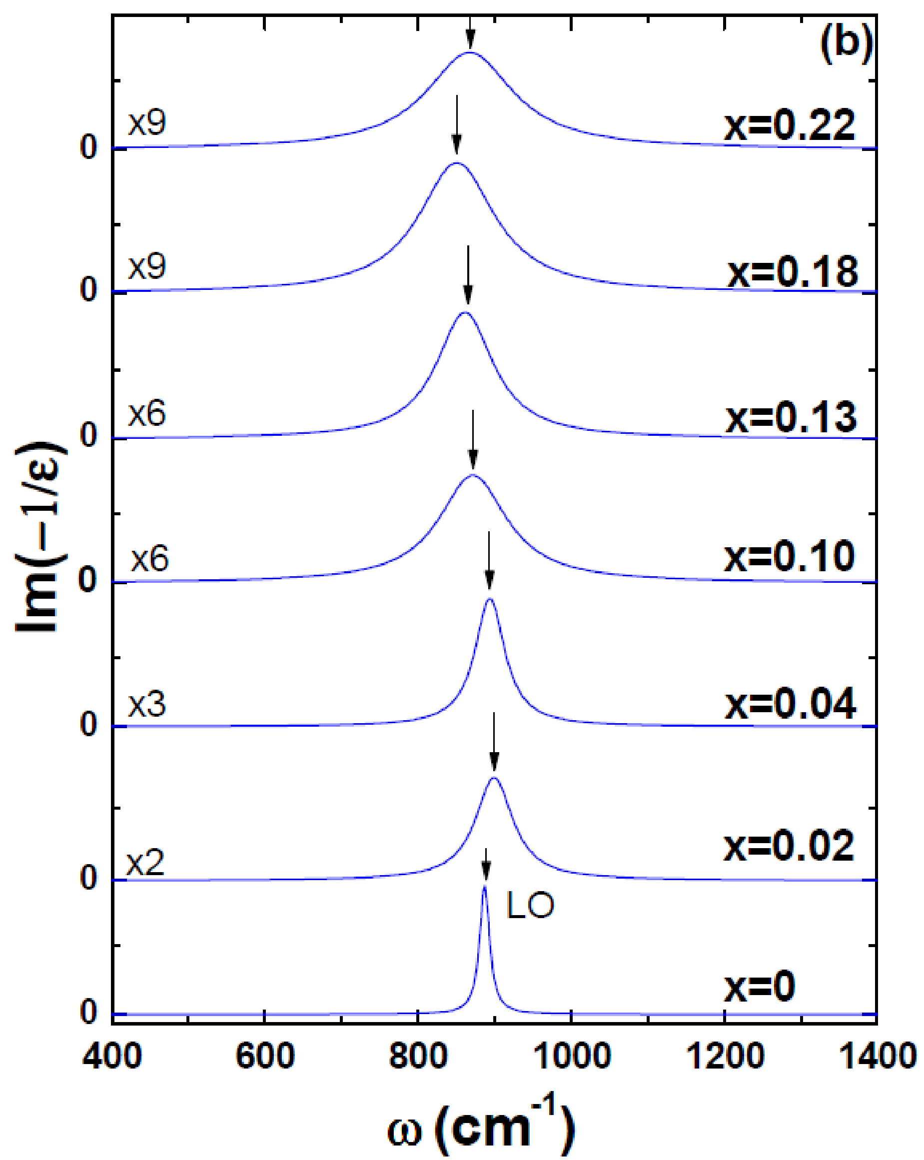

Fig. 3 (b)

Fig. 4: Raman scattering spectra for the $Y_xAl_{1-x}N$ layers $0 \leq x \leq 0.10$, the asterisks indicate the sapphire vibrational modes, inset: E_2 (high) vibration mode.

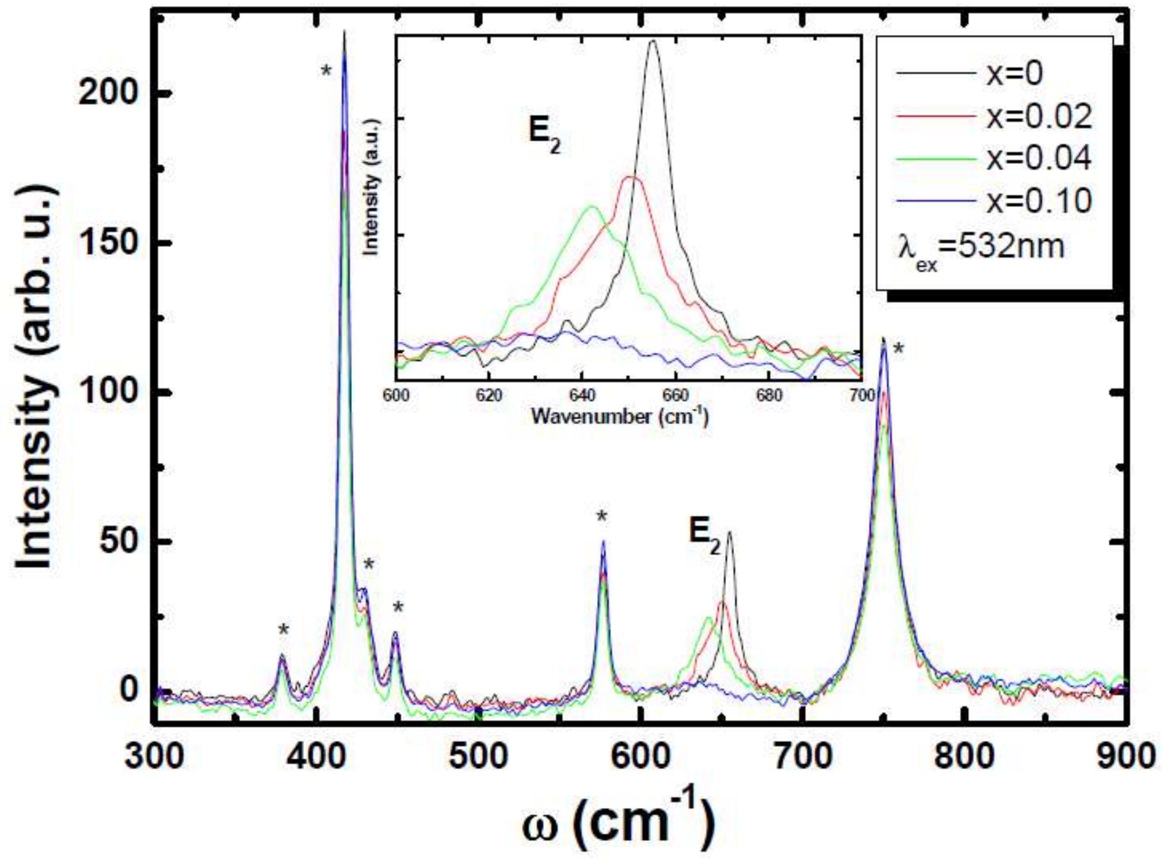

Fig. 5: $Y_xAl_{1-x}N$ optical phonon frequencies obtained from the IRSE data analysis (LO and E_1(TO)) and Raman scattering measurements (E_2), as function of yttrium content x.

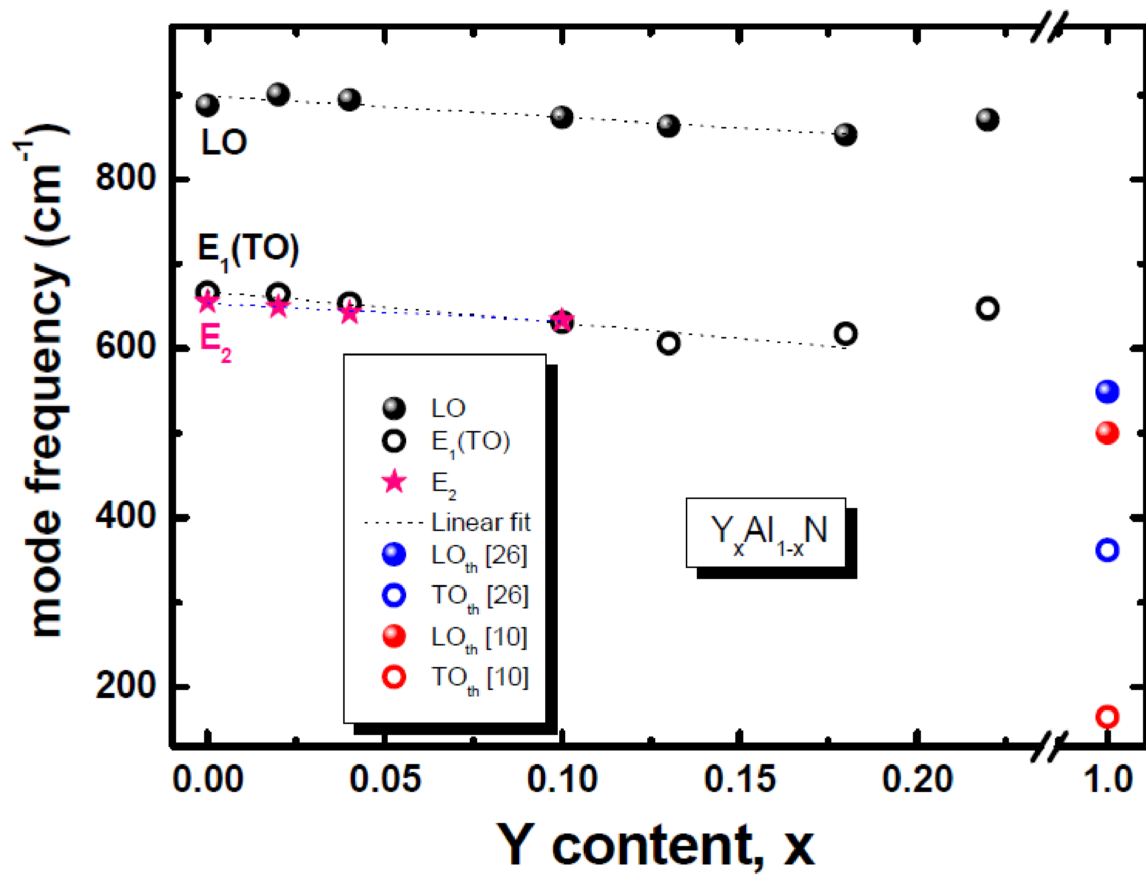

Fig. 6: High-frequency limit dielectric constant ε_∞ obtained from the IRSE analysis, static dielectric constant ε_0 calculated from Lyddane-Sachs-Teller relation, and calculated Born effective charge Z_B, as function of yttrium content x for $Y_xAl_{1-x}N$.